



1 **Black carbon variability since preindustrial times in Eastern**
2 **part of Europe reconstructed from Mt Elbrus, Caucasus ice**
3 **cores**

4 Saehee Lim^{1,*}, Xavier Faïn¹, Patrick Ginot^{1,2}, Vladimir Mikhaleiko³, Stanislav Kutuzov³,
5 Jean-Daniel Paris⁴, Anna Kozachek³ and Paolo Laj^{1,2}

6 ¹ Univ. Grenoble-Alpes, CNRS, Institut des Géosciences de l'Environnement, Grenoble, France.

7 ² Univ. Grenoble-Alpes, CNRS, IRD, Observatoire des Sciences de l'Univers, Grenoble, France.

8 ³ Institute of Geography, Russian Academy of Sciences, Moscow, Russia.

9 ⁴ Laboratoire des Sciences du Climat et de l'Environnement, IPSL, CEA-CNRS-UVSQ, CE Orme des Merisiers,
10 91190 Gif sur Yvette, France.

11 *now at: Department of Earth and Environmental Sciences, Korea University, Seoul, South Korea.

12 *Corresponding to:* S. Lim (saehee.lim@gmail.com)

13 **Abstract** Black carbon (BC), emitted by fossil fuel combustion and biomass burning, is the second largest man-
14 made contributor to global warming after carbon dioxide (Bond et al., 2013). However, limited information
15 exists on its past emissions and atmospheric variability. In this study, we present the first high-resolution record
16 of refractory BC (rBC, including mass concentration and size) reconstructed from ice cores drilled at a high-
17 altitude Eastern European site in Mt. Elbrus (ELB), Caucasus (5115 m a.s.l.). The ELB ice core record, covering
18 the period 1825-2013, reflects the atmospheric load of rBC particles at the ELB site transported from the
19 European continent with a larger rBC input from sources located in the Eastern part of Europe. In the first half of
20 the 20th century, European anthropogenic emissions resulted in a 1.5-fold increase in the ice core rBC mass
21 concentrations as respect to its level in the preindustrial era (before 1850). The rBC mass concentrations
22 increased by a 5-fold in 1960-1980, followed by a decrease until ~2000. Over the last decade, the rBC signal for
23 summer time slightly increased. We have compared the signal with the atmospheric BC load simulated using
24 past BC emissions (ACCMIP and MACCity inventories) and taken into account the contribution of different
25 geographical region to rBC distribution and deposition at the ELB site. Interestingly, the observed rBC
26 variability in the ELB ice core record since the 1960s is not in perfect agreement with the simulated atmospheric
27 BC load. Similar features between the ice core rBC record and the best scenarios for the atmospheric BC load
28 support that anthropogenic BC increase in the 20th century is reflected in the ELB ice core record. However, the
29 peak in BC mass concentration observed in ~1970 in the ice core is estimated to occur a decade later from past
30 inventories. BC emission inventories for the period 1960s-1970s may be underestimating European
31 anthropogenic emissions. Furthermore, for summer time snow layers of the last 2000s, the slightly increasing
32 trend of rBC deposition likely reflects recent changes in anthropogenic and biomass burning BC emissions in the
33 Eastern part of Europe. Our study highlights that the past changes in BC emissions of Eastern Europe need to be
34 considered in assessing on-going air quality regulation.

35 **1 Introduction**

36 Climate forcing of black carbon (BC), a primary aerosol emitted by fossil fuel and biomass combustions, is of



37 great concern due to its strong light-absorbing ability and small size allowing it to transport over long distances
38 (Bond et al., 2013; Ramanathan and Carmichael, 2008). In high-altitude or –latitude areas, BC has been
39 identified as a significant contributor that may accelerate snowmelt (Hansen and Nazarenko, 2004; Xu et al.,
40 2016). Despite numerous studies through both measurements and model simulations (Bond et al., 2013 and
41 references therein), little is known about BC’s past variability, e.g., before year 2000, and sensitivity to climate
42 change primarily due to limited in-situ atmospheric BC measurements both temporally and spatially (Collaud
43 Coen et al., 2007, 2013).

44 Reconstruction of atmospheric BC variability from ice core archives can thereby be very helpful to understand
45 past BC emissions and provide additional constraint on BC emission inventories (Bisiaux et al., 2012a; Kaspari
46 et al., 2011; Legrand et al., 2007; McConnell et al., 2007; Wang et al., 2015). Particularly, the geographical
47 proximity of the ice cores at high-altitude Alpine sites, e.g., European Alpine sites such as Col du Dôme, Colle
48 Gnifetti and Fiescherhorn (Jenk et al., 2006; Legrand et al., 2013; Thevenon et al., 2009) to densely populated
49 regions allows us to observe a fingerprint of BC emissions and past temporal variability in the anthropogenic
50 source regions. In this respect, elemental carbon (EC) records reconstructed from ice cores at Western European
51 Alpine sites (Col du Dôme and Colle Gnifetti) highlight a pronounced EC increase starting mid-20th century
52 (Legrand et al., 2007; Thevenon et al., 2009) with increasing anthropogenic activity in the Western Europe
53 (Fagerli et al., 2007; Lamarque et al., 2010). However, recent EC records over the last two decades are not
54 available from these Western European ice cores, which makes it difficult to quantify historic BC emissions and
55 thus provide implications for assessing European air quality regulation initiated since 1970 (Tørseth et al., 2012;
56 Vestreng et al., 2007). Furthermore, long-term ice core BC records have never been reconstructed from the
57 Eastern European regions where even atmospheric measurements are relatively scarce (Pio et al., 2007; Yttri et
58 al., 2007). Reconstruction of BC records with a wide range of coverage both temporally and spatially is crucial
59 to understand BC emission properties and establish regulations on the emissions.

60 In this study, we present a high-resolution record of refractory BC (rBC) deposition to snow at a high-altitude
61 site in Mt. Elbrus, Caucasus (5115 m a.s.l.) covering the period 1825-2013. Located between the Black and the
62 Caspian seas, Mt. Elbrus is influenced by prevailing westerly from the European continent (Mikhaleenko et al.,
63 2015). The ice core rBC record, that is reconstructed in the downstream of European continent, therefore
64 provides information on long-term variability and evolution of BC emissions of Europe. The study documents
65 the variability of rBC deposition and provides a comparison with the expected atmospheric BC variability based
66 on past emission inventories also considering atmospheric transport to the drilling site.

67

68 **2. Method**

69 **2.1 Ice core drilling site**

70 A 181.8 m-long ice core (the 2009 core) was drilled at the Western Plateau of Mt. Elbrus (ELB), the highest
71 summit of the Caucasus (43°20′53,9″N, 42°25′36,0″E, 5115 m a.s.l.) (Figure 1) on September 2009. In addition,
72 a 20.4 m-long ice core (the 2013 core) was extracted in June 2013 at the same site to expand the existing ice-core
73 sample set from 2009 to 2013. Drilling was performed in a dry borehole with a lightweight electromechanical
74 drilling system, and was accompanied by borehole temperature measurements. Borehole temperatures ranged
75 from -17 °C to 10 m depth to -2.4 °C at 181 m of the 2009 core (Mikhaleenko et al., 2015).



76 The core were packed in polyethylene sealed bag and stored on the glacier at -10°C . After the drilling campaign,
77 the core were packed in insulated core boxes and shipped frozen to the cold laboratory of the Lomonosov
78 Moscow State University for preliminary investigation and water stable isotopes analyzes. In Moscow, the core
79 was split and one-half was shipped to LGGE (Laboratoire de Glaciologie et Géophysique de l'Environnement -
80 now Institut de Géophysique de l'Environnement) in Grenoble, France for additional analyzes.

81

82 2.2 rBC ice core analysis

83 The top 156.6 m of the 2009 core and the entire 2013 core were analyzed at LGGE in 2013-2014 and in 2014,
84 respectively, using an ice core melter system coupled with a jet nebulizer (APEX-Q, Elemental Scientific Inc.,
85 Omaha, NE) and a single particle soot photometer (SP2, Droplet Measurement Technologies, Boulder,
86 Colorado). We have used the terminology proposed by Petzold et al. (2013) for incandescence-based BC
87 measurements. Our results are therefore reported in terms of refractory-BC (rBC). It should be noted that there is
88 a direct relationship (although not necessarily linear) between rBC and BC measured with other techniques
89 (Kondo et al., 2011a; Laborde et al., 2012; Miyakawa et al., 2016).

90 Dust and conductivity are continuously analyzed simultaneously to rBC. Briefly, ice core sticks (3.4 cm x 3.4
91 cm x 1 m) were melted at a mean rate of 3 cm min^{-1} and the melt water from the inner 6.8 cm^2 of the sticks were
92 continuously collected. After de-bubbling, the sample flow is split to rBC analytical line with a mean flow of
93 about $70\pm 10\text{ }\mu\text{L min}^{-1}$. The flow rate dedicated to rBC analyses is continuously recorded using a mass flow meter
94 (SENSIRION© SLI-2000). In parallel, the melt water was sampled by two auto-samplers at the end of the CFA
95 for off-line ionic species analysis and archive storage. The upper section of the 2009 firn core was analyzed
96 discretely.

97 Ice core rBC analysis using the SP2 has been reported previously (Bisiaux et al., 2012a, 2012b; Ginot et al.,
98 2014; Jenkins et al., 2013; Kaspari et al., 2014; Wang et al., 2015). Specifically, recent papers describe detailed
99 analytical evaluation for rBC in liquid samples, e.g., rain, snow and ice core, using the SP2 (Lim et al., 2014;
100 Mori et al., 2016; Schwarz et al., 2012; Wendl et al., 2014). The SP2 uses a laser-induced incandescence method
101 to measure the mass of individual rBC particle (Schwarz et al., 2006; Stephens et al., 2003). Briefly, an
102 individual rBC particle passes through the laser beam intra-cavity of a 1,064 nm Nd YAG laser and
103 incandescences. Of two PMT-photo detectors (broad and narrow bands) that are used to detect incandescence
104 signal, we used only broadband detector to derive rBC mass avoiding low signal-to-noise ratio from the
105 narrowband detector. The SP2 was calibrated by analyzing mass-selected fullerene soot (Alfa Aesar Inc., USA).
106 The design and gain settings of our SP2 resulted in the lower and upper limit of measurements for rBC mass to
107 be $\sim 0.3\text{-}220\text{ fg}$. A particle larger than 220 fg was treated as the particle of 220 fg. Loss of rBC particles occurring
108 during aerosolization in the APEX-Q was calibrated and corrected daily by rBC standard solutions (Aquadag®,
109 Acheson Inc., USA; 8 steps from 0.1 to $100\text{ }\mu\text{g L}^{-1}$), which resulted in rBC mass recovery of $75\pm 7\%$. The rBC
110 fraction that was not aerosolized was partially identified in drains and internal surface of the APEX-Q (see
111 Supplementary information in Lim et al. (2014)). To prevent contamination and achieve the rBC levels as low as
112 possible, both an instrumental blank (ultrapure water) and a 5-cm procedure blank (frozen ultrapure water cut in
113 the cold room) were run daily prior to field sample analysis, until the rBC counting reached 0 to 1 per second,
114 equivalent to rBC concentration of less than $0.01\text{ }\mu\text{g L}^{-1}$.



115 High resolution continuous rBC data recorded every second was smoothed at a depth resolution of 1 cm, except
116 the upper section (surface to 7.2 m depth) of the 2009 core that was discretely analyzed at a depth resolution of
117 ~5-10 cm. The density of rBC data points per year depends on annual snow accumulation rates and ice thinning
118 with depth. The two ice cores are overlap for snow layers of year 2007-2009 (Fig. S1). The records described
119 here for rBC concentrations are (i) the 2009 ice core from 2.9 m to 156.6 m, corresponding to calendar years of
120 1825-2008 and (ii) the top 15.9 m of the 2013 core, corresponding to calendar years of 2009-2013. These two ice
121 core records cover the calendar years of 1825-2013.

122 As a first survey for long-term rBC size distributions of ice core record, mass equivalent diameter of measured
123 single rBC, D_{rBC} , was calculated, assuming a void-free BC density of 1.8 g cm^{-3} (Moteki and Kondo, 2010). The
124 calculated D_{rBC} was in the range of ~70 and 620 nm. A series of test using mono-dispersed polystyrene latex
125 (PSL) spheres with known diameters (150-600 nm) and poly-dispersed standard BC (Aquadag®) suggests that
126 the APEX-Q/SP2 system preserves original size information of rBC particles in liquid samples and provides
127 highly reproducible rBC size measurements with a variation of < 5 nm (Sect. 2.2.3 and 2.2.5 in Lim et al., 2014;
128 Wendl et al., 2014). rBC size distributions were retrieved seasonally and simplified with a log-normal fit with a
129 bin size (#)=200. Mass mode diameter (MMD) of the log-normal fit was then extracted to further reduce
130 parameters. Size intervals between bin channels vary, with the minimum interval of less than 8 nm for the MMD
131 200-350 nm. Here, all SP2 data were processed with the SP2 toolkit developed by M. Gysel at the Paul Scherrer
132 Institute (PSI, Switzerland; <http://aerosolsoftware.web.psi.ch/>).

133

134 2.3 Ice core dating and seasonal signature

135 Ice core dating was determined by counting annual layers from 1825 to 2013 using the seasonal cycles of
136 ammonium, succinic acid and water stable isotopes (δD and $\delta^{18}\text{O}$) that were analyzed discretely. Based on the
137 examination of the ammonium and succinic acid profiles, each annual layer was divided into two parts
138 corresponding to snow deposition under winter condition and summer condition (Legrand et al., 2013; Preunkert
139 et al., 2000). In addition, the annual layer counting was further confirmed using the reference horizon from a
140 tritium peak (1963) and a volcanic horizon (Katmai in 1912). The mean annual net accumulation rate of 1455
141 mm w.e. for the last 140 years was estimated from these proxies. The dating uncertainty is likely on the order of
142 a few years due to ice thinning with deeper depths. Further details about dating are found in Mikhalenko et al.
143 (2015).

144 Ice core seasonality was determined by the ammonium stratigraphy and further verified by the isotope variations.
145 However, seasonal separation of the high-resolution rBC record made by lower-resolution ammonium profile
146 was sometimes challenging particularly at the edge of two seasons, misleading winter (summer) rBC layers to be
147 more concentrated (less concentrated) by the adjacent seasonal rBC layer. To avoid inaccurate separation of an
148 annual ice layer into winter and summer intervals, only mid-summer and mid-winter rBC concentrations were
149 extracted by considering data comprised between the 25th percentile and the 75th percentile of the depth thickness
150 of each seasonal snow layer. The mid-summer and mid-winter are therefore corresponding roughly to the
151 warmest three months and the coldest three months (“background winter”) of a year. Later in the manuscript,
152 summer and winter of this study will refer to mid-summer and mid-winter, respectively.

153



154 2.4 Atmospheric transport modeling

155 2.4.1 Model description and runs

156 FLEXPART v6.2 lagrangian particle dispersion model (LPDM) calculates the trajectories of tracer particles
157 using the mean winds interpolated from the gridded analysis field and parameterizations representing turbulence
158 and convective transport (Forster et al., 2007; Stohl and Thomson, 1999). FLEXPART was run using reanalysis
159 fields of the European Centre for Medium-Range Weather Forecasts (ECMWF, ERA-Interim) at $0.75^{\circ} \times 0.75^{\circ}$
160 resolution, which is available since 1979. Here, a backward simulation mode was used to analyze particles
161 transport pathways from potential flux regions to the sampling site (Seibert and Frank, 2004; Stohl et al., 2005).

162 To limit computational cost, simulations were performed for two selected periods: 2005-2009 and 1979-1983.
163 We selected these periods because: (i) year 1979 is the first year of ECMWF data and year 2009 is the last year
164 of our longer ice core (2009 ice core) that were analyzed prior to the 2013 ice core and (ii) these years are
165 inflections in rBC trends (Sect. 3.2). It would thus be sufficient to analyze transport patterns influencing rBC at
166 ELB and determine potential changes in these transport patterns. 1,000 particles are released at the drilling site
167 during every 5-day interval in June to August (JJA) and in December to February (DJF). Modelled global
168 average atmospheric lifetimes of BC particles varies by a factor of more than 3, ranging from 3 to 10 days (Bond
169 et al., 2013). Because BC particles reaching the high-altitude ELB site would experience longer lifetimes than
170 the particles transporting in the planetary boundary layer (PBL), simulations were performed using a BC lifetime
171 of 5-, and 7-day. However, 7-day air mass trajectories were extending to the Pacific and therefore made little
172 difference with the 5 days simulations. Thus we set the BC lifetime as 5-day. Number of particles were then
173 computed every 3h at $0.5^{\circ} \times 0.5^{\circ}$ resolution.

174

175 2.4.2 Sensitivity by potential source regions

176 The finally defined footprint density $F(i, j, n)$ is expressed as a parameter encompassing released particle
177 number and residence time along the particles pathway, in procedure defined unit (p.d.u.). This final result is
178 theoretically identical to potential emission sensitivity (PES), called source-receptor-relationship by Seibert and
179 Frank (2004), which is proportional to the particle residence time in a particular grid cell with a fixed altitude
180 range.

181 To facilitate analysis we reduced the number of variables from the gridded footprint density by summing them
182 over large regions. We classified the footprint areas into five geographical regions with specific rBC emission
183 sources (Figure 2). The regions identified are as follows: **EEU** (Eastern Europe including nearby the Mt. Elbrus,
184 Ukraine and Europe Russia and a part of Middle East), **CEU** (Central Europe), **WEU** (Western Europe), **NAF**
185 (North Africa), **NAM** (North America) and **Others** (The Atlantic and a part of Northern Europe above 60°N).

186 To display our results, we first calculate the footprint density F_e of the entire footprint area:

$$187 F_e(i, j) = \sum_{n=1}^N F(i, j, n)$$

188 Here, $F(i, j, n)$ is footprint density, where i and j are the indices of the latitude/longitude grid and n runs over the
189 total number of cases N . F_e indicates the entire footprint area where the aerosols track during the last 5 days of
190 transport. Note that we found little inter-annual variability in the footprint contribution of each region to the ELB
191 site with a 3 % variation over the two periods (2005-2009 and 1979-1983). Assuming that this inter-annual



192 variability in footprint density is not large enough to influence on long-term rBC trends and the results over the
193 two periods are thus fairly representative of 20th century, we combined the simulations results and used this
194 approach to study long-term emission contribution of each geographical region to rBC distribution and
195 deposition at our drilling site.

196 In addition to the calculation using total particles in the atmospheric column, calculations using particles
197 positioned in the lowest 2 km layers in the atmosphere were performed to investigate emission source regions of
198 aerosols transporting from low altitudes. To show the potential particle transport strength of each region relative
199 to the entire area, we calculated the percentages of the footprint density in each region relative to the one in the
200 entire area. To do this, we sum $F_e(i, j)$ over the entire footprint area resulting in one value. In the same way, we
201 sum $F(i, j)$ within each of the five regions resulting in five values.

202

203 2.5 Historic BC emission inventories

204 To describe temporal variability in the regional BC emissions and atmospheric load of BC transported to the
205 ELB site, we used time-varying anthropogenic and biomass burning BC emissions estimated by ACCMIP
206 (Emissions for Atmospheric Chemistry and Climate Model Intercomparison Project) inventory for the period
207 1900-2000 on the decadal scale (at 0. 5°×0. 5° resolution; Lamarque et al., 2010) and MACCity
208 (MACC/CityZEN EU projects) inventory for the year 2008 (at 0. 5°×0. 5° resolution; Diehl et al., 2012; Granier
209 et al., 2011; Lamarque et al., 2010; van der Werf et al., 2006). Note that the ACCMIP inventory provide decadal
210 means (e.g., '1980' corresponds to the mean of 1980-1989) for the biomass burning estimates and representative
211 values (e.g., '1980' is a representative of 1975-1985) for the anthropogenic estimates, leading to 5-year shift
212 between two estimates. We used anthropogenic emission only for constraining BC emissions in DJF and both
213 anthropogenic and biomass burning emissions for constraining BC emissions in JJA, because biomass burning
214 frequently occurs in summer time as respect to anthropogenic emissions occurring year-round.

215 3 Results and discussion

216 3.1 High resolution rBC record from Elbrus ice cores

217 We present the first high-resolution rBC record of ice cores drilled in the Mt. Elbrus, Caucasus (2009 and 2013
218 cores, Figure 3a). The rBC concentrations along the two cores ranged from 0.01 $\mu\text{g L}^{-1}$ to 222.2 $\mu\text{g L}^{-1}$ with a
219 mean $\pm 1\sigma$ of 11.0 ± 11.3 $\mu\text{g L}^{-1}$ and a median of 7.2 $\mu\text{g L}^{-1}$. A 20-m long section is zoomed in Figure 3b to
220 highlight the higher resolution of rBC signals when continuously recorded at 1-cm depth interval compared to
221 the surface snow and firn section (from top to 6.1 m) analyzed discretely at ~5-10 cm-depth interval. The rBC
222 record was found to preserve sub-annual variability from top to depth of 156.6 m with rBC spikes reflecting
223 large and abrupt variability in deposition of atmospheric rBC particles. Such high-resolution record brings new
224 opportunities to study dynamic atmospheric vertical transport and/or sporadic events in a season.

225 A well-marked seasonal rBC cycle (e.g., Fig 3b) was characterized for the 2013 core and the 2009 core down to
226 156.6 m by consistent high summer values ranging from 0.2 to 222.2 $\mu\text{g L}^{-1}$ with a mean $\pm 1\sigma$ of 15.5 ± 12.9 $\mu\text{g L}^{-1}$
227 and a median of 11.7 $\mu\text{g L}^{-1}$ and low winter values ranging from 0.2 to 44.6 $\mu\text{g L}^{-1}$ with a mean $\pm 1\sigma$ of 5.9 ± 5.1
228 $\mu\text{g L}^{-1}$ and a median of 4.5 $\mu\text{g L}^{-1}$ (Table 1). Peak rBC mass concentration of an annual snow layer was observed



229 in summer snow layer. In atmospheric observations at ground-based sites in Western and Central Europe
230 boundary layer, EC aerosol mass concentrations in winter are higher roughly by a factor of 2 than in summer
231 mainly due to the enhanced domestic heating (Pio et al., 2007; Tsyro et al., 2007). In contrast to the boundary
232 layer sites, the atmospheric measurements at high-elevation sites in Europe (e.g., Puy de Dôme at 1465 m a.s.l.
233 and Sonnblick at 3106 m a.s.l.) revealed 2 to 3 times higher EC levels during summer than winter (Pio et al.,
234 2007; Venzac et al., 2009), reflecting the efficient upward transport of BC aerosols from the polluted boundary
235 layer to the high-altitudes during summer, primarily by thermally-driven convection and thickening boundary-
236 layer height (Lugauer et al., 1998; Matthias and Bösenberg, 2002). This is consistent to the rBC seasonality
237 observed in the ELB ice core.
238

239 3.2 Long term evolution of rBC mass concentrations

240 Time series of summer and winter medians of rBC mass concentrations from 1825 to 2013 are shown in Figure
241 4. Medians are shown with lower and upper 10th percentiles to illustrate seasonal rBC concentrations. The rBC
242 concentrations varied significantly over the past ~190 years with a large inter-annual variability. Both summer
243 and winter rBC medians increased gradually since the onset of 20th century with a rapid increase in ~1950 lasting
244 until ~1980. Median concentrations reached their maximums in the mid-1960s for summer (37.5 $\mu\text{g L}^{-1}$) and in
245 the late 1970s for winter (14.7 $\mu\text{g L}^{-1}$).

246 Concentrations and relative change to levels of preindustrial era (here, defined as 1825-1850) for given time
247 periods are summarized in Table 1. For the period of 1825-1850, median (\pm standard deviation, SD) of rBC
248 concentrations were $4.3 \pm 1.5 \mu\text{g L}^{-1}$ in summer and $2.0 \pm 0.9 \mu\text{g L}^{-1}$ in winter. The rBC concentrations increased by
249 a ~1.5-fold in 1900-1950. Over the period of 1960-1980, rBC concentrations increased by a factor of 5.0 in
250 summer and a factor of 3.3 in winter. The larger relative change of summer rBC than one of winter for the period
251 suggests that rBC emissions in summer source region increased more sharply for this time period. Notably, in
252 addition to medians, the lower 10th percentiles of both summer and winter rBC increased since the preindustrial
253 era, highlighting that rBC background level in the atmosphere at ELB was also significantly modified.
254 Meanwhile, upper 10th percentiles ranged up to 75 $\mu\text{g L}^{-1}$ and 35 $\mu\text{g L}^{-1}$ for summer and winter, respectively.

255 Of the EC records available in the Western European mountain glaciers, only Col du Dôme (hereafter, CDD;
256 Legrand et al., 2007) and Colle Gnifetti (hereafter, CG; Thevenon et al., 2009) summer records provide EC
257 records for the recent time (until ~1990 and 1980, respectively), whereas the Fiescherhorn (hereafter, FH; Jenk
258 et al., 2006) record is available until 1940 only. Both summer records at CDD and CG show somewhat comparable
259 preindustrial EC levels (~2 $\mu\text{g L}^{-1}$ for CDD and ~7 $\mu\text{g L}^{-1}$ for CG in the mid-1800s) to the ELB rBC ($4.3 \pm 1.5 \mu\text{g}$
260 L^{-1} in 1825-1850) and substantially increased EC concentrations for the period 1950-1980 since the mid-19th
261 century, similar to the ELB rBC. This suggests that EC emissions show a common trend at the European scale,
262 and that such trend has been recorded in the different European high-altitude ice cores from CDD, CG, and ELB.
263 Some differences, such as peak time period and increase/decrease rate between records that may reflect sub-
264 regional (e.g., Western Europe vs. Eastern Europe) emission changes, may be also noteworthy. However, direct
265 comparison of the ELB rBC with the Western European ice core records should be made with caution owing to
266 both (i) different analytical methods applied for the ice cores (e.g., ELB rBC: APEX-Q/SP2, CDD EC: thermal-
267 optical method with EUSAAR2 protocol, and CG EC: thermal method) and (ii) lower data resolution particularly



268 for the CDD core (a few data points for a decadal EC concentration). We thus focus on evaluating the ELB rBC
269 record in Sect. 3.5 by comparing with simulated atmospheric load of BC particles that were transported from
270 source regions to the Mt. Elbrus.

271

272 3.3 Past variability in rBC size distributions

273 The first record of temporal and seasonal changes in rBC size distribution was extracted from the ELB ice core.
274 Mass equivalent diameter of rBC particles (D_{rBC}) was log-normally distributed. The mode of rBC mass size
275 distributions (mass mode diameter, MMD) was determined for both summer and winter layers by fitting a log-
276 normal curve to the measured distribution (e.g., Figure S2). This approach provides reliable results of
277 representative rBC size in seasonal ice layers as the determined MMDs fall into the measured size range (~70-
278 620 nm).

279 Figure 5 shows time series of rBC MMD for the period of 1940 to 2009. The upper and lower limits of the
280 periods selected for retrieving rBC MMD were chosen so as a large number of rBC particles in the seasonal ice
281 layer would be available and would allow to secure reliable size distribution of the ice layer. Faster melting of
282 snow layers of year 2010-2013 and thinner ice layers below the layer of year 1940 did not allow to record
283 sufficient numbers of rBC particles and thus robust rBC size distributions could not be retrieve. For the
284 considered time period, rBC MMD of both summer and winter layers varied ranging from 207.3 nm to 378.3 nm
285 with a geometric mean of 279.4 ± 1.1 nm. No clear temporal change in rBC MMD was identified over the 1940-
286 2009 period.

287 Notably, rBC particles measured in this study show the MMD shifted to larger sizes than those measured in the
288 atmosphere over Europe (MMD of 130-260 nm) (Dahlkötter et al., 2014; Laborde et al., 2013; Liu et al., 2010;
289 McMeeking et al., 2010; Reddington et al., 2013), even larger than atmospheric rBC diameter measured at an
290 high alpine site, Jungfrauoch (JFJ) in Switzerland (MMD of 220-240 nm) (Liu et al., 2010). The shift of rBC
291 sizes induced by dry deposition should be negligible, as wet deposition with fairly constant precipitation
292 throughout the year (e.g., 52% in summer and 48% in winter of annual mean precipitation at Pereval
293 Klukhorskij observatory located at 2037 m a.s.l. in the Western Caucasus) is the dominant aerosol removal
294 pathway at this site (Mikhaleenko et al., 2015). Similarly, significant snow melt was not observed in the ELB
295 summer ice layers and post-deposition processes are thus not expected to alter rBC size distributions. Rather, the
296 different rBC size distributions of the ice core from those in the atmosphere are likely associated with removal
297 process of rBC particles during precipitation. Recent study using the SP2 technique showed the rBC size
298 distribution in rainwater shifted to larger sizes (MMD= ~200 nm) than that in air (MMD= ~150 nm) in Tokyo,
299 indicating that large rBC particles were more efficiently removed by precipitation (Mori et al., 2016). The
300 preferential wet removal of larger rBC particles (Mori et al., 2016; Moteki et al., 2012) could reasonably explain
301 the larger MMD of rBC particles observed in the ice core than atmospheric rBC aerosols (Schwarz et al., 2013).

302 The seasonal variations in rBC size distribution are clearly visible. In summer, the MMD varied ranging from
303 227.4 nm to 378.3 nm with a geometric mean of 290.8 ± 1.1 nm (Fig.5, red curve). In winter, the MMD varied
304 ranging from 207.3 nm to 344.9 nm with a geometric mean of 268.7 ± 1.1 nm (Fig.5, blue curve). The rBC MMD
305 of summer ice layers tended to be slightly larger than that of winter layers. Despite few observational evidences,
306 we hypothesize that larger rBC size in summer may reflect advection of rBC aerosols transported from the PBL



307 by thermally-driven convection, while in winter aerosols transported in the free troposphere (FT) could be
308 smaller due to longer residence time in the atmosphere and accordingly, more chances for larger aerosols to be
309 removed by precipitation prior to reaching the ELB site. Our hypothesis seems to be reasonable being consistent
310 to the findings of in-situ aerosol measurements at high-altitude sites in Europe. Liu et al. (2010) found that rBC
311 aerosols at JFJ were slightly larger when the site was influenced by valley sources, anthropogenic pollutants
312 from lower altitudes. Submicron aerosol size distributions were also overall shifted to larger size in summer (50
313 to 150 nm) than in winter (below 50 nm) at European mountain stations with altitude of ~1000-3000 m a.s.l.
314 (Asmi et al., 2011). The authors in the latter explained this feature by relatively polluted air masses from the PBL
315 during daytime in summer, but more influence of the FT air masses in winter. Similar to the clear seasonal cycle
316 in rBC mass concentration, the clear seasonal rBC size distributions of the ELB ice core point out seasonal
317 differences in origins of air masses reaching the ELB drilling site: PBL air with less chance of aerosol wet
318 removal in summer and the free tropospheric air in winter.

319 In addition, the larger rBC MMD in summer layers can be associated with specific summer sources of
320 atmospheric rBC particles, such as forest fires and/or agricultural fires. Particularly, forest fires in Southern
321 Europe and agricultural fires in Eastern Europe may well contribute to summer aerosol loading in Europe
322 (Bovchaliuk et al., 2013; van der Werf et al., 2010; Yoon et al., 2011). Previous SP2 studies have reported the
323 larger size of rBC aerosols for biomass burning plumes, e.g., MMD of ~200 nm (Kondo et al., 2011b; Schwarz et
324 al., 2008; Taylor et al., 2014) compared to rBC sizes for urban plumes. In the ELB ice core, we observed a
325 maximum rBC MMD of 378.3 nm, with a maximum rBC mass concentration of 222.2 $\mu\text{g L}^{-1}$ in the late summer
326 snow layer of year 2003, when extreme forest fire events occurred over the Iberian Peninsula and the
327 Mediterranean coast (Barbosa et al., 2004; Hodzic et al., 2006) resulting from a record-breaking heatwave in
328 Europe (Luterbacher et al., 2004; Schär et al., 2004). Both forward and backward air mass trajectories calculated
329 from HYSPLIT model support that the ELB site was potentially influenced by the intense forest fires occurred in
330 the Southern part of Europe on the mid-August 2003 (Fig. S3), when the top altitude of the PBL was estimated to
331 be ~4.5 km high (Hodzic et al., 2006). Although speculative, this snow layer of year 2003 peaked with rBC
332 concentration and enriched with larger-sizes rBC particles indicates potential contribution of biomass burning
333 aerosols transported westerly to the ELB site.

334 The rBC size distributions preserved in Elbrus cores could be discussed as an influence of seasonal vertical
335 transport versus emission sources of rBC aerosols and their wet removal properties. This rBC size information is
336 potential to provide important implications particularly for the determination of snow-melting potential by rBC
337 particles in snow (Flanner et al., 2007; Schwarz et al., 2013). Comparison of rBC size with well-established
338 biomass burning proxies would be required to better characterize the dependency of rBC sizes with past fire
339 activities.

340

341 3.4 Potential emission source regions

342 Figure 6 illustrates potential source regions of BC aerosols reaching the ELB site. The model results show that
343 relative to the footprints in JJA, footprints in DJF were more spread out of European continent and extended
344 further over the Pacific (Figure 6a and b). The relative contributions of each regional footprint density over the
345 total density are summarized in Fig. 7. Most of aerosols reaching the ELB site are transported from the European



346 continent (WEU+CEU+EEU) accounting for 71.0 % and 55.6 % in JJA and DJF, respectively. The region EEU
347 brings the greatest contribution with fairly consistent features for both seasons, accounting for 35.6 % and
348 30.9 % in JJA and DJF, respectively. A stronger seasonality was found in the region NAF and the region NAM,
349 where the footprint contribution was larger in DJF by a 2-fold. This seasonal variation is caused by longer
350 particle trajectories promoted by a faster zonal flow in winter across the North Atlantic from west to east.

351 To investigate contributions of aerosols transporting from low altitudes which may reflect emissions at surface
352 more sensitively, we calculated the footprint density of particles positioned in the lowest 2 km layers in the
353 atmosphere. Note that we arbitrarily selected this vertical height of atmosphere (2 km layer) since particles
354 positioned at lower atmosphere (e.g., ~1 km layer) was rarely observed in our simulations and the PBL heights
355 were often higher in European mountains up to 3 km (Matthias, 2004). The results for JJA show that unlike in
356 the entire atmospheric column, the contribution of footprint density from the region EEU was almost doubled in
357 the 2 km layer, accounting for 63.6 % (Fig. 6c). Contrarily, in DJF, the proportion of the region EEU was only
358 22 % over total footprint density in this fixed layer. We thus infer that large seasonal increases observed during
359 summer time in rBC mass concentration are likely driven by deposition of rBC aerosols transported from Eastern
360 part of Europe and mostly originating from lower altitudes.

361 Therefore, these FLEXPART results confirm that rBC deposition to the Mt. Elbrus is most likely dominated by
362 transport of BC emissions from the European continent, with the strongest BC inputs from the Eastern part of
363 Europe particularly in summer.

364

365 **3.5 New constrains on European BC emissions**

366 Refractory BC concentrations of the ELB ice core increased rapidly from the 1950s to the 1980s (Figure 4 in
367 Sect. 3.2), and such trend record should primarily reflect changes in European BC emissions (Sect. 3.4). Here,
368 we compare past emission BC inventories with the ELB ice core record to bring new constrains on past
369 European BC emissions.

370 Figure 8 shows temporal changes in anthropogenic and biomass burning BC emissions for the period 1900-2008
371 estimated by ACCMIP and MACCity (Diehl et al., 2012; Granier et al., 2011; Lamarque et al., 2010; van der
372 Werf et al., 2006). The overall emission trends (black lines) illustrate a decrease of anthropogenic emissions
373 since 1900 (Figure 8a) and a high variability of biomass burning emissions over the whole period (Figure 8b).
374 For anthropogenic emissions, the largest BC emissions in EEU and CEU regions occurred in 1980, followed by
375 decreasing trends. WEU had the strongest BC emissions lasting until 1960, followed by a decrease of BC
376 emissions lasting the present-day. In 2008, anthropogenic BC emissions in region EEU, CEU and WEU are
377 comparable with an order of 0.2 Tg yr^{-1} .

378 To investigate factors controlling long-term rBC trends preserved in the ELB ice core, the temporal evolution of
379 measured ice core rBC particles can be directly compared with that of atmospheric BC load at the ELB site, at
380 least in relative manner. This comparison is provided in Fig. 9, in which ice core record is averaged along a
381 decadal scale to be comparable with the historic BC emission data available on decadal scale only (Lamarque et
382 al., 2010). Specifically, we coupled the BC emission intensities in each region and their relative contribution to
383 the entire footprint area of ELB site (Figure 8c and d). The decadal BC emission burden in each region (Figure
384 8a and b) is therefore multiplied by the contribution of footprint density (Figure 7). Assumption behind this



385 comparison is that (i) the atmospheric circulation and transport patterns do not change with time and (ii) that the
386 mechanisms for BC depositing to snow remained constant. Hence, the proportionality between BC mass
387 concentration in snow and atmospheric BC load has not varied with time.

388 For summertime (JJA case, Fig. 9a) optimal agreement in trend pattern is observed between the ice core rBC
389 and the atmospheric BC estimated in the lower 2 km layer with an increase at the onset of the 20th century and a
390 subsequent decrease since ~1980 (“best scenario”). Specifically, substantial increase in atmospheric BC load is
391 observed for the period 1910-1970, similar to the ELB rBC ice core record, only when the atmospheric BC
392 considers BC particles transported in the lowest 2 km layer of the atmosphere. On the other side, the estimation
393 derived from the entire atmospheric column does exhibit a different pattern. This comparison indicates that
394 changes primarily in European anthropogenic BC emissions (e.g., industry, traffic and residential combustion),
395 particularly ones of Eastern part of Europe, are consequently reflected in the ELB ice core rBC variability over
396 the last century.

397 For wintertime (DJF case, Fig. 9b), the ice core rBC variability before 1980 can be explained by the atmospheric
398 BC load (anthropogenic only) in the entire atmospheric column but without North American (NAM)
399 contribution. With NAM contribution included in the simulation, the atmospheric BC is overestimated before
400 1980 resulting in a flat or a slightly downward trend for the period 1910-1970, unlike to the ice core rBC trend.
401 However, the good agreement between long-term rBC changes of Greenland ice core and modeled BC
402 deposition in Greenland using a chemistry-climate model with an input of ACCMIP BC inventory confirm that
403 BC emission estimates for NAM from the ACCMIP inventory correctly quantify anthropogenic BC emissions in
404 North America (Lamarque et al., 2010). Consequently, the observed overestimation of NAM contribution for
405 winter at the ELB site (Fig 9b) is likely due to an overestimation of NAM footprint density in the statistical
406 process applied on FLEXPART simulation data. Finally, the estimated BC without NAM contribution is defined
407 as the “best scenario” for winter time.

408 Despite the similar features between the ice core rBC record and the best scenario for the atmospheric load
409 which support that anthropogenic BC increase in the 20th century is reflected in the ELB record, BC maximum
410 time period is not in total agreement (Fig. 9a and b). Unlike the ice core rBC that already largely increased in
411 1960 and peaked in 1970 for both summer and winter, the atmospheric BC load remarkably increases only in
412 1980. Substantial BC increase of ELB and Western European (CDD and CG) ice cores since the mid-20th
413 century reveals that BC emissions increased during that period at a wide regional European scale. In addition, the
414 CDD record shows a large increase in sulfate concentration since the mid-20th century lasting until ~1980
415 (Preunkert and Legrand, 2013; Preunkert et al., 2001). Knowing that sulfate and BC are often co-emitted in
416 anthropogenic emission sources, e.g., in industrial sectors, one can expect a large increase in European BC
417 emissions in 1960-1980, as suggested by the ELB ice core rBC record. The reliability of historic emission
418 inventories for BC is reported to be lower than for SO₂, CO and NO_x emissions, particularly for the period prior
419 to 2000 (Granier et al., 2011), which is due to the uncertainties on BC emission factors for coal, gasoline and
420 diesel fuels in various sectors (differ by a factor of 10 or more in literatures) and activity data (Granier et al.,
421 2011; Vignati et al., 2010). Thus, the lack of substantial increase in the atmospheric BC load for the period
422 1960s-1970s could be associated primarily with underestimated European anthropogenic BC emissions for this
423 period (Fig. 8c and d).

424 Moreover, the ice core rBC record and the atmospheric BC load do not exhibit similar patterns after 1980.



425 Decreasing rates of the ice core rBC are much slower after 1980 onward for both seasons than the atmospheric
426 BC load (Fig. 9a and b). Furthermore, the summer rBC trend of the ELB ice core even increased since 2000,
427 although such a trend cannot be reported conclusively for winter layers (Fig. 4). The recent economic growth in
428 Eastern, and some part of Central, European countries (World Bank Group, 2016) can contribute to the
429 enhancement in the release of BC and co-emitted pollutants. Some of Eastern European countries have kept
430 increasing their sulfur emissions mainly from heat production and public electricity from 2000 onward (Vestreng
431 et al., 2007). Thus, the increase in rBC deposition at the Elbrus site, mostly identified in summer, was probably
432 related to enhanced emissions from anthropogenic sources located in Eastern and Central Europe. On the other
433 side, many of Eastern European countries, such as Ukraine and European part Russia which are geographically
434 close to the Mt. Elbrus, are the countries with the greatest land use for agriculture in Europe (Rabbinge and van
435 Diepen, 2000), and thus emissions of smoke aerosols from their agricultural waste burning are expected to be
436 significant in summer time (Barnaba et al., 2011; Bovchaliuk et al., 2013; Stohl et al., 2007). Large emissions of
437 smoke aerosols over Eastern Europe from summer forest/agricultural fires have been recently reported (Barnaba
438 et al., 2011; Bovchaliuk et al., 2013; Sciare et al., 2008; Yoon et al., 2011; Zhou et al., 2012) and burned area
439 from Global Fire Emissions Database (GFED) (Giglio et al., 2010) increased over Eastern Europe for the period
440 2004-2008 (Yoon et al., 2014). These emissions of smoke aerosols in the Eastern part of Europe may have
441 contributed to the observed summer BC increase in the ELB ice cores. Thus, the recent trend of the ELB ice core
442 rBC turning upward probably indicates changes in both anthropogenic emissions and summer forest/peat fires
443 over Eastern part of Europe in 2000s, which is not well reflected in the inventories.

444 Given the large existing uncertainties in historic BC emission inventories available to date, our rBC record
445 reconstructed from a high-altitude Caucasus ice cores should be useful to better constrain BC emissions.
446 Specifically, our study highlights the need for improving BC emission inventories from the Eastern part of
447 Europe since 1960. Reliability of Western European BC emissions could be more specifically assessed by
448 investigating high-resolution BC records extracted from Western European ice cores that would be more
449 representative of Western European emissions.

450

451 **4 Conclusions**

452 A high-resolution rBC record reconstructed from ice cores drilled from a high-altitude Eastern European site in
453 Mt. Elbrus (ELB), Caucasus, reported for the first time the long-term evolutions of rBC mass concentrations and
454 size distributions in the European outflows over the past 189 years, i.e., between year 1825 and year 2013. The
455 rBC record at ELB is largely impacted by rBC emissions located in the Eastern part of Europe. A large temporal
456 variability in rBC mass concentration was observed at both seasonal and annual timescales. This record is also
457 unique to document long-term variability of BC in this region of Europe.

458 In the first-half of 20th century, rBC concentrations increased by a 1.5-fold than its level in the preindustrial era
459 (before 1850). The rBC concentrations increased by a 5-fold in 1960-1980, followed by a decrease until ~2000
460 and a slight increase again since ~2000. Consistent increase in background levels, since the beginning of 20th
461 century, highlights that rBC background level in the atmosphere at ELB was also significantly altered. We have
462 also investigated the potential of size distributions of rBC particles in the ice cores as new a proxy to bring
463 additional information on rBC removal processes, seasonal transport patterns, and emission sources.



464 We simulated the atmospheric load of BC aerosols which were transported from the European continent, mainly
465 Eastern part of Europe, by coupling transport simulations (FLEXPART) to 20th-century BC emission inventories
466 (ACCMIP and MACCity). Similar features were observed between the ELB ice core rBC mass concentration
467 record and the best scenario for the atmospheric BC load at the ELB site: a BC increase at the onset of the 20th
468 century and a subsequent decrease since ~1980. This estimation evidently supports that European anthropogenic
469 activities resulted in the BC increase over Europe since ~1900, which was also seen in elemental carbon (EC)
470 records of Western European ice cores (Legrand et al., 2007; Thevenon et al., 2009). However, some
471 disagreements were seen between the ELB ice core rBC and the best scenario for atmospheric BC load at ELB,
472 e.g., (i) the lack of strong increase in the best scenario for the period 1960s and 1970s, unlike the ice core record,
473 (ii) the different decreasing rates after 1980 and (iii) the slightly increasing trend of the rBC ELB ice core record
474 that was not shown in the estimation. An explanation for such discrepancy could be that rapid enhancement of
475 BC emissions over Europe since 1960 and the recent BC changes in the Eastern part of Europe may not be well
476 accounted for in the emission inventories.

477 Most atmospheric BC measurements have focused on western and northern Europe (e.g., McMeeking et al.,
478 2010; Reche et al., 2011; Reddington et al., 2013) despite of growing evidences of strong aerosol emissions in
479 the Eastern part of Europe (Asmi et al., 2011; Barnaba et al., 2011; Bovchaliuk et al., 2013). It is thus critically
480 important to deploy new studies (atmospheric monitoring and investigation of ice archives) with a more
481 comprehensive European view, including both Western and Eastern areas. We suggest that century-long ice cores
482 at multiple high-altitude European sites with a homogeneous or well crossed- compared measurement techniques
483 are needed to better constrain past BC emissions, infer efficiency of present BC emission regulation, and help
484 establishing future regulations on BC emissions.

485

486 **Acknowledgments**

487 This work was supported by the PEGASOS project funded by the European Commission under the Framework
488 Programme 7 (FP7-ENV-2010-265148) and by the Russian Foundation for Basic Research (RFBR) grants 07-
489 05-00410 and 09-05-10043. This work received funding from the French ANR programs RPD COCLICO
490 (ANR-10-RPDOC-002-01) and the European Research Council under the European Community's Seventh
491 Framework Program FP7/2007–2013 Grant Agreement n° 291062 (project ICE&LASERS). S. Lim
492 acknowledges support of the Korean Ministry of Education and Science Technology through a government
493 scholarship and of the Basic Science Research Program through the National Research Foundation of Korea
494 (NRF) funded by the Ministry of Education (2015R1A6A3A01061393). V. Mikhalenko and S. Kutuzov
495 acknowledge support of the Russian Academy of Sciences (Department of Earth Sciences ONZ-12 Project) and
496 RFBR grant 14-05-00137. Grateful thank to M. Zanatta for technical help in SP2 operation, S. Preunkert for
497 technical help in ice core cutting, M. Legrand for helpful discussions, A. Berchet and J-L Bonne for help in
498 FLEXPART simulations and N. Kehrwald for analytical help.

499

500 **References**

501 Asmi, A., Wiedensohler, A., Laj, P., Fjaeraa, A.-M., Sellegri, K., Birmili, W., Weingartner, E., Baltensperger, U.,
502 Zdimal, V., Zikova, N., Putaud, J.-P., Marinoni, A., Tunved, P., Hansson, H.-C., Fiebig, M., Kivekäs, N.,
503 Lihavainen, H., Asmi, E., Ulevicius, V., Aalto, P. P., Swietlicki, E., Kristensson, A., Mihalopoulos, N., Kalivitis,



- 504 N., Kalapov, I., Kiss, G., de Leeuw, G., Henzing, B., Harrison, R. M., Beddows, D., O'Dowd, C., Jennings, S. G.,
505 Flentje, H., Weinhold, K., Meinhardt, F., Ries, L. and Kulmala, M.: Number size distributions and seasonality of
506 submicron particles in Europe 2008–2009, *Atmos. Chem. Phys.*, 11(11), 5505–5538, doi:10.5194/acp-11-5505-
507 2011, 2011.
- 508 Barbosa, P., San-Miguel-Ayanz, J., Camia, A., Gimeno, M., Liberta, G. and Schmuck, G.: Assessment of fire
509 damages in the EU Mediterranean Countries during the 2003 Forest Fire Campaign, Official Publication of the
510 European Commission, Ispra., 2004.
- 511 Barnaba, F., Angelini, F., Curci, G. and Gobbi, G. P.: An important fingerprint of wildfires on the European
512 aerosol load, *Atmos. Chem. Phys.*, 11(20), 10487–10501, doi:10.5194/acp-11-10487-2011, 2011.
- 513 Bisiaux, M. M., Edwards, R., McConnell, J. R., Curran, M. A. J., Van Ommen, T. D., Smith, A. M., Neumann, T.
514 A., Pasteris, D. R., Penner, J. E. and Taylor, K.: Changes in black carbon deposition to Antarctica from two
515 high-resolution ice core records, 1850–2000 AD, *Atmos. Chem. Phys.*, 12(9), 4107–4115, doi:10.5194/acp-12-
516 4107-2012, 2012a.
- 517 Bisiaux, M. M., Edwards, R., McConnell, J. R., Albert, M. R., Anschutz, H., Neumann, T. A., Isaksson, E. and
518 Penner, J. E.: Variability of black carbon deposition to the East Antarctic Plateau, 1800–2000 AD, *Atmos. Chem.*
519 *Phys.*, 12(8), 3799–3808, doi:10.5194/acp-12-3799-2012, 2012b.
- 520 Bond, T. C., Doherty, S. J., Fahey, D. W., Forster, P. M., Berntsen, T., DeAngelo, B. J., Flanner, M. G., Ghan, S.,
521 Kärcher, B., Koch, D., Kinne, S., Kondo, Y., Quinn, P. K., Sarofim, M. C., Schultz, M. G., Schulz, M.,
522 Venkataraman, C., Zhang, H., Zhang, S., Bellouin, N., Guttikunda, S. K., Hopke, P. K., Jacobson, M. Z., Kaiser,
523 J. W., Klimont, Z., Lohmann, U., Schwarz, J. P., Shindell, D., Storelvmo, T., Warren, S. G. and Zender, C. S.:
524 Bounding the role of black carbon in the climate system: A scientific assessment, *J. Geophys. Res. Atmos.*,
525 118(11), 5380–5552, doi:10.1002/jgrd.50171, 2013.
- 526 Bovchaliuk, A., Milinevsky, G., Danylevsky, V., Goloub, P., Dubovik, O., Holdak, A., Ducos, F. and Sosenkin,
527 M.: Variability of aerosol properties over Eastern Europe observed from ground and satellites in the period from
528 2003 to 2011, *Atmos. Chem. Phys.*, 13(13), 6587–6602, doi:10.5194/acp-13-6587-2013, 2013.
- 529 Dahlkötter, F., Gysel, M., Sauer, D., Minikin, A., Baumann, R., Seifert, P., Ansmann, A., Fromm, M., Voigt, C.
530 and Weinzierl, B.: The Pagami Creek smoke plume after long-range transport to the upper troposphere over
531 Europe – aerosol properties and black carbon mixing state, *Atmos. Chem. Phys.*, 14(12), 6111–6137,
532 doi:10.5194/acp-14-6111-2014, 2014.
- 533 Diehl, T., Heil, A., Chin, M., Pan, X., Streets, D., Schultz, M. and Kinne, S.: Anthropogenic, biomass burning,
534 and volcanic emissions of black carbon, organic carbon, and SO₂ from 1980 to 2010 for hindcast model
535 experiments, *Atmos. Chem. Phys. Discuss.*, 12(9), 24895–24954, doi:10.5194/acpd-12-24895-2012, 2012.
- 536 Fagerli, H., Legrand, M., Preunkert, S., Vestreng, V., Simpson, D. and Cerqueira, M.: Modeling historical long-
537 term trends of sulfate, ammonium, and elemental carbon over Europe: A comparison with ice core records in the
538 Alps, *J. Geophys. Res.*, 112(D23), D23S13, doi:10.1029/2006JD008044, 2007.
- 539 Flanner, M. G., Zender, C. S., Randerson, J. T. and Rasch, P. J.: Present-day climate forcing and response from
540 black carbon in snow, *J. Geophys. Res.*, 112(D11), doi:Artn D11202 Doi 10.1029/2006jd008003, 2007.
- 541 Forster, C., Stohl, A. and Seibert, P.: Parameterization of Convective Transport in a Lagrangian Particle
542 Dispersion Model and Its Evaluation, *J. Appl. Meteorol. Climatol.*, 46(4), 403–422, doi:10.1175/JAM2470.1,
543 2007.



- 544 Giglio, L., Randerson, J. T., van der Werf, G. R., Kasibhatla, P. S., Collatz, G. J., Morton, D. C. and DeFries, R.
545 S.: Assessing variability and long-term trends in burned area by merging multiple satellite fire products,
546 *Biogeosciences*, 7(3), 1171–1186, doi:10.5194/bg-7-1171-2010, 2010.
- 547 Ginot, P., Dumont, M., Lim, S., Patris, N., Taupin, J.-D., Wagnon, P., Gilbert, A., Arnaud, Y., Marinoni, A.,
548 Bonasoni, P. and Laj, P.: A 10 year record of black carbon and dust from a Mera Peak ice core (Nepal):
549 variability and potential impact on melting of Himalayan glaciers, *Cryosph.*, 8(4), 1479–1496, doi:10.5194/tc-8-
550 1479-2014, 2014.
- 551 Granier, C., Bessagnet, B., Bond, T. C., D'Angiola, A., Denier van der Gon, H., Frost, G. J., Heil, A., Kaiser, J.
552 W., Kinne, S., Klimont, Z., Kloster, S., Lamarque, J.-F., Liousse, C., Masui, T., Meleux, F., Mieville, A., Ohara,
553 T., Raut, J.-C., Riahi, K., Schultz, M. G., Smith, S. J., Thompson, A., Aardenne, J., Werf, G. R. and Vuuren, D.
554 P.: Evolution of anthropogenic and biomass burning emissions of air pollutants at global and regional scales
555 during the 1980–2010 period, *Clim. Change*, 109(1-2), 163–190, doi:10.1007/s10584-011-0154-1, 2011.
- 556 Guilhermet, J., Preunkert, S., Voisin, D., Baduel, C. and Legrand, M.: Major 20th century changes of water-
557 soluble humic-like substances (HULIS WS) aerosol over Europe inferred from Alpine ice cores, *J. Geophys.*
558 *Res. Atmos.*, 118(9), 3869–3878, doi:10.1002/jgrd.50201, 2013.
- 559 Hansen, J. and Nazarenko, L.: Soot climate forcing via snow and ice albedos, *Proc. Natl. Acad. Sci. U. S. A.*,
560 101(2), 423–428, doi:DOI 10.1073/pnas.2237157100, 2004.
- 561 Hodzic, A., Vautard, R., Chepfer, H., Goloub, P., Menut, L., Chazette, P., Deuzé, J. L., Apituley, A. and Couvert,
562 P.: Evolution of aerosol optical thickness over Europe during the August 2003 heat wave as seen from
563 CHIMERE model simulations and POLDER data, *Atmos. Chem. Phys.*, 6(7), 1853–1864, doi:10.5194/acp-6-
564 1853-2006, 2006.
- 565 Jenk, T. M., Szidat, S., Schwikowski, M., Gaggeler, H. W., Brutsch, S., Wacker, L., Synal, H. A. and Saurer, M.:
566 Radiocarbon analysis in an Alpine ice core: record of anthropogenic and biogenic contributions to carbonaceous
567 aerosols in the past (1650-1940), *Atmos. Chem. Phys.*, 6, 5381–5390, doi:10.5194/acp-6-5381-2006, 2006.
- 568 Jenkins, M., Kaspari, S., Kang, S., Grigholm, B. and Mayewski, P. A.: Black carbon concentrations from a
569 Tibetan Plateau ice core spanning 1843–1982: recent increases due to emissions and glacier melt, *Cryosph.*
570 *Discuss.*, 7(5), 4855–4880, doi:10.5194/tcd-7-4855-2013, 2013.
- 571 Kaspari, S., Painter, T. H., Gysel, M., Skiles, S. M. and Schwikowski, M.: Seasonal and elevational variations of
572 black carbon and dust in snow and ice in the Solu-Khumbu, Nepal and estimated radiative forcings, *Atmos.*
573 *Chem. Phys.*, 14(15), 8089–8103, doi:10.5194/acp-14-8089-2014, 2014.
- 574 Kaspari, S. D., Schwikowski, M., Gysel, M., Flanner, M. G., Kang, S., Hou, S. and Mayewski, P. A.: Recent
575 increase in black carbon concentrations from a Mt. Everest ice core spanning 1860-2000 AD, *Geophys. Res.*
576 *Let.*, 38, doi:Artn L04703 Doi 10.1029/2010gl046096, 2011.
- 577 Kondo, Y., Sahu, L., Moteki, N., Khan, F., Takegawa, N., Liu, X., Koike, M. and Miyakawa, T.: Consistency
578 and Traceability of Black Carbon Measurements Made by Laser-Induced Incandescence, Thermal-Optical
579 Transmittance, and Filter-Based Photo-Absorption Techniques, *Aerosol Sci. Technol.*, 45(2), 295–312,
580 doi:10.1080/02786826.2010.533215, 2011a.
- 581 Kondo, Y., Matsui, H., Moteki, N., Sahu, L., Takegawa, N., Kajino, M., Zhao, Y., Cubison, M. J., Jimenez, J. L.,
582 Vay, S., Diskin, G. S., Anderson, B., Wisthaler, A., Mikoviny, T., Fuelberg, H. E., Blake, D. R., Huey, G.,
583 Weinheimer, A. J., Knapp, D. J. and Brune, W. H.: Emissions of black carbon, organic, and inorganic aerosols



- 584 from biomass burning in North America and Asia in 2008, *J. Geophys. Res.*, 116(D8), D08204,
585 doi:10.1029/2010JD015152, 2011b.
- 586 Laborde, M., Schnaiter, M., Linke, C., Saathoff, H., Naumann, K.-H., Möhler, O., Berlenz, S., Wagner, U.,
587 Taylor, J. W., Liu, D., Flynn, M., Allan, J. D., Coe, H., Heimerl, K., Dahlkötter, F., Weinzierl, B., Wollny, A. G.,
588 Zanatta, M., Cozic, J., Laj, P., Hitzenberger, R., Schwarz, J. P. and Gysel, M.: Single Particle Soot Photometer
589 intercomparison at the AIDA chamber, *Atmos. Meas. Tech.*, 5, 3077–3097, doi:10.5194/amt-5-3077-2012, 2012.
- 590 Laborde, M., Crippa, M., Tritscher, T., Jurányi, Z., Decarlo, P. F., Temime-Roussel, B., Marchand, N., Eckhardt,
591 S., Stohl, A., Baltensperger, U., Prévôt, A. S. H., Weingartner, E. and Gysel, M.: Black carbon physical
592 properties and mixing state in the European megacity Paris, *Atmos. Chem. Phys.*, 13(11), 5831–5856,
593 doi:10.5194/acp-13-5831-2013, 2013.
- 594 Lamarque, J.-F., Bond, T. C., Eyring, V., Granier, C., Heil, A., Klimont, Z., Lee, D., Liousse, C., Mieville, A.,
595 Owen, B., Schultz, M. G., Shindell, D., Smith, S. J., Stehfest, E., Van Aardenne, J., Cooper, O. R., Kainuma, M.,
596 Mahowald, N., McConnell, J. R., Naik, V., Riahi, K. and van Vuuren, D. P.: Historical (1850–2000) gridded
597 anthropogenic and biomass burning emissions of reactive gases and aerosols: methodology and application,
598 *Atmos. Chem. Phys.*, 10(15), 7017–7039, doi:10.5194/acp-10-7017-2010, 2010.
- 599 Lavanchy, V. M. H., Gäggeler, H. W., Schotterer, U., Schwikowski, M. and Baltensperger, U.: Historical record
600 of carbonaceous particle concentrations from a European high-alpine glacier (Colle Gnifetti, Switzerland), *J.*
601 *Geophys. Res. Atmos.*, 104(D17), 21227–21236, doi:10.1029/1999jd900408, 1999.
- 602 Legrand, M., Preunkert, S., Schock, M., Cerqueira, M., Kasper-Giebl, A., Afonso, J., Pio, C., Gelencsér, A. and
603 Dombrowski-Etchevers, I.: Major 20th century changes of carbonaceous aerosol components (EC, WinOC,
604 DOC, HULIS, carboxylic acids, and cellulose) derived from Alpine ice cores, *J. Geophys. Res.*, 112(D23),
605 D23S11, doi:10.1029/2006jd008080, 2007.
- 606 Legrand, M., Preunkert, S., May, B., Guilhermet, J., Hoffman, H. and Wagenbach, D.: Major 20th century
607 changes of the content and chemical speciation of organic carbon archived in Alpine ice cores: Implications for
608 the long-term change of organic aerosol over Europe, *J. Geophys. Res. Atmos.*, 118(9), 3879–3890,
609 doi:10.1002/jgrd.50202, 2013.
- 610 Lim, S., Faïn, X., Zanatta, M., Cozic, J., Jaffrezo, J.-L., Ginot, P. and Laj, P.: Refractory black carbon mass
611 concentrations in snow and ice: method evaluation and inter-comparison with elemental carbon measurement,
612 *Atmos. Meas. Tech.*, 7(10), 3307–3324, doi:10.5194/amt-7-3307-2014, 2014.
- 613 Liu, D., Flynn, M., Gysel, M., Targino, A., Crawford, I., Bower, K., Choularton, T., Jurányi, Z., Steinbacher, M.,
614 Hüglin, C., Curtius, J., Kampus, M., Petzold, A., Weingartner, E., Baltensperger, U. and Coe, H.: Single particle
615 characterization of black carbon aerosols at a tropospheric alpine site in Switzerland, *Atmos. Chem. Phys.*,
616 10(15), 7389–7407, doi:10.5194/acp-10-7389-2010, 2010.
- 617 Lugauer, M., Baltensperger, U., Furger, M., Gäggeler, H. W., Jost, D. T., Schwikowski, M. and Wanner, H.:
618 Aerosol transport to the high Alpine sites Jungfraujoch (3454 m asl) and Colle Gnifetti (4452 m asl), *Tellus B*,
619 50(1), doi:10.3402/tellusb.v50i1.16026, 1998.
- 620 Luterbacher, J., Dietrich, D., Xoplaki, E., Grosjean, M. and Wanner, H.: European seasonal and annual
621 temperature variability, trends, and extremes since 1500., *Science*, 303(5663), 1499–503,
622 doi:10.1126/science.1093877, 2004.
- 623 Matthias, V. and Bösenberg, J.: Aerosol climatology for the planetary boundary layer derived from regular lidar



- 624 measurements, *Atmos. Res.*, 63(3-4), 221–245, doi:10.1016/S0169-8095(02)00043-1, 2002.
- 625 McConnell, J. R., Edwards, R., Kok, G. L., Flanner, M. G., Zender, C. S., Saltzman, E. S., Banta, J. R., Pasteris,
626 D. R., Carter, M. M. and Kahl, J. D. W.: 20th-century industrial black carbon emissions altered arctic climate
627 forcing, *Science* (80-.), 317(5843), 1381–1384, doi:10.1126/science.1144856, 2007.
- 628 McMeeking, G. R., Hamburger, T., Liu, D., Flynn, M., Morgan, W. T., Northway, M., Highwood, E. J., Krejci,
629 R., Allan, J. D., Minikin, A. and Coe, H.: Black carbon measurements in the boundary layer over western and
630 northern Europe, *Atmos. Chem. Phys.*, 10(19), 9393–9414, doi:10.5194/acp-10-9393-2010, 2010.
- 631 Mikhaleenko, V., Sokratov, S., Kutuzov, S., Ginot, P., Legrand, M., Preunkert, S., Lavrentiev, I., Kozachek, A.,
632 Ekaykin, A., Faïn, X., Lim, S., Schotterer, U., Lipenkov, V. and Toropov, P.: Investigation of a deep ice core
633 from the Elbrus western plateau, the Caucasus, Russia, *Cryosph.*, 9(6), 2253–2270, doi:10.5194/tc-9-2253-2015,
634 2015.
- 635 Miyakawa, T., Kanaya, Y., Komazaki, Y., Taketani, F., Pan, X., Irwin, M. and Symonds, J.: Intercomparison
636 between a single particle soot photometer and evolved gas analysis in an industrial area in Japan: Implications
637 for the consistency of soot aerosol mass concentration measurements, *Atmos. Environ.*, 127, 14–21,
638 doi:10.1016/j.atmosenv.2015.12.018, 2016.
- 639 Mori, T., Moteki, N., Ohata, S., Koike, M., Goto-Azuma, K., Miyazaki, Y. and Kondo, Y.: Improved technique
640 for measuring the size distribution of black carbon particles in liquid water, *Aerosol Sci. Technol.*, 50(3), 242–
641 254, doi:10.1080/02786826.2016.1147644, 2016.
- 642 Moteki, N. and Kondo, Y.: Dependence of Laser-Induced Incandescence on Physical Properties of Black Carbon
643 Aerosols: Measurements and Theoretical Interpretation, *Aerosol Sci. Technol.*, 44(8), 663–675,
644 doi:10.1080/02786826.2010.484450, 2010.
- 645 Moteki, N., Kondo, Y., Oshima, N., Takegawa, N., Koike, M., Kita, K., Matsui, H. and Kajino, M.: Size
646 dependence of wet removal of black carbon aerosols during transport from the boundary layer to the free
647 troposphere, *Geophys. Res. Lett.*, 39(13), doi:10.1029/2012GL052034, 2012.
- 648 Petzold, A., Ogren, J. A., Fiebig, M., Laj, P., Li, S.-M., Baltensperger, U., Holzer-Popp, T., Kinne, S.,
649 Pappalardo, G., Sugimoto, N., Wehrli, C., Wiedensohler, A. and Zhang, X.-Y.: Recommendations for reporting
650 “black carbon” measurements, *Atmos. Chem. Phys.*, 13(16), 8365–8379, doi:10.5194/acp-13-8365-2013, 2013.
- 651 Pio, C. A., Legrand, M., Oliveira, T., Afonso, J., Santos, C., Caseiro, A., Fialho, P., Barata, F., Puxbaum, H.,
652 Sanchez-Ochoa, A., Kasper-Giebl, A., Gelencsér, A., Preunkert, S. and Schock, M.: Climatology of aerosol
653 composition (organic versus inorganic) at nonurban sites on a west-east transect across Europe, *J. Geophys. Res.*,
654 112(D23), D23S02, doi:10.1029/2006JD008038, 2007.
- 655 Preunkert, S. and Legrand, M.: Towards a quasi-complete reconstruction of past atmospheric aerosol load and
656 composition (organic and inorganic) over Europe since 1920 inferred from Alpine ice cores, *Clim. Past*, 9(4),
657 1403–1416, doi:10.5194/cp-9-1403-2013, 2013.
- 658 Preunkert, S., Wagenbach, D., Legrand, M. and Vincent, C.: Col du Dôme (Mt Blanc Massif, French Alps)
659 suitability for ice-core studies in relation with past atmospheric chemistry over Europe, *Tellus B*, 52(3), 993–
660 1012, doi:10.1034/j.1600-0889.2000.d01-8.x, 2000.
- 661 Preunkert, S., Legrand, M. and Wagenbach, D.: Sulfate trends in a Col du Dôme (French Alps) ice core: A
662 record of anthropogenic sulfate levels in the European midtroposphere over the twentieth century, *J. Geophys.*
663 *Res. Atmos.*, 106(D23), 31991–32004, doi:10.1029/2001JD000792, 2001.



- 664 Rabbinge, R. and van Diepen, C. A.: Changes in agriculture and land use in Europe, *Eur. J. Agron.*, 13(2-3), 85–
665 99, doi:10.1016/S1161-0301(00)00067-8, 2000.
- 666 Ramanathan, V. and Carmichael, G.: Global and regional climate changes due to black carbon, *Nat. Geosci.*, 1(4),
667 221–227, 2008.
- 668 Reche, C., Querol, X., Alastuey, A., Viana, M., Pey, J., Moreno, T., Rodríguez, S., González, Y., Fernández-
669 Camacho, R., de la Rosa, J., Dall’Osto, M., Prévôt, A. S. H., Hueglin, C., Harrison, R. M. and Quincey, P.: New
670 considerations for PM, Black Carbon and particle number concentration for air quality monitoring across
671 different European cities, *Atmos. Chem. Phys.*, 11(13), 6207–6227, doi:10.5194/acp-11-6207-2011, 2011.
- 672 Reddington, C. L., McMeeking, G., Mann, G. W., Coe, H., Frontoso, M. G., Liu, D., Flynn, M., Spracklen, D. V.
673 and Carslaw, K. S.: The mass and number size distributions of black carbon aerosol over Europe, *Atmos. Chem.*
674 *Phys.*, 13(9), 4917–4939, doi:10.5194/acp-13-4917-2013, 2013.
- 675 Schär, C., Vidale, P. L., Lüthi, D., Frei, C., Häberli, C., Liniger, M. A. and Appenzeller, C.: The role of
676 increasing temperature variability in European summer heatwaves., *Nature*, 427(6972), 332–6,
677 doi:10.1038/nature02300, 2004.
- 678 Schwarz, J. P., Gao, R. S., Fahey, D. W., Thomson, D. S., Watts, L. a., Wilson, J. C., Reeves, J. M., Darbeheshti,
679 M., Baumgardner, D. G., Kok, G. L., Chung, S. H., Schulz, M., Hendricks, J., Lauer, a., Kärcher, B., Slowik, J.
680 G., Rosenlof, K. H., Thompson, T. L., Langford, a. O., Loewenstein, M. and Aikin, K. C.: Single-particle
681 measurements of midlatitude black carbon and light-scattering aerosols from the boundary layer to the lower
682 stratosphere, *J. Geophys. Res.*, 111(D16), D16207, doi:10.1029/2006JD007076, 2006.
- 683 Schwarz, J. P., Gao, R. S., Spackman, J. R., Watts, L. A., Thomson, D. S., Fahey, D. W., Ryerson, T. B., Peischl,
684 J., Holloway, J. S., Trainer, M., Frost, G. J., Baynard, T., Lack, D. A., de Gouw, J. A., Warneke, C. and Del
685 Negro, L. A.: Measurement of the mixing state, mass, and optical size of individual black carbon particles in
686 urban and biomass burning emissions, *Geophys. Res. Lett.*, 35(13), L13810, doi:10.1029/2008GL033968, 2008.
- 687 Schwarz, J. P., Doherty, S. J., Li, F., Ruggiero, S. T., Tanner, C. E., Perring, A. E., Gao, R. S. and Fahey, D. W.:
688 Assessing Single Particle Soot Photometer and Integrating Sphere/Integrating Sandwich Spectrophotometer
689 measurement techniques for quantifying black carbon concentration in snow, *Atmos. Meas. Tech.*, 5(11), 2581–
690 2592, doi:10.5194/amt-5-2581-2012, 2012.
- 691 Schwarz, J. P., Gao, R. S., Perring, A. E., Spackman, J. R. and Fahey, D. W.: Black carbon aerosol size in snow.,
692 *Sci. Rep.*, 3, 1356, doi:10.1038/srep01356, 2013.
- 693 Sciare, J., Oikonomou, K., Favez, O., Markaki, Z., Liakakou, E., Cachier, H. and Mihalopoulos, N.: Long-term
694 measurements of carbonaceous aerosols in the eastern Mediterranean: evidence of long-range transport of
695 biomass burning, *Atmos. Chem. Phys. Discuss.*, 8(2), 6949–6982, doi:10.5194/acpd-8-6949-2008, 2008.
- 696 Seibert, P. and Frank, a.: Source-receptor matrix calculation with a Lagrangian particle dispersion model in
697 backward mode, *Atmos. Chem. Phys.*, 4(1), 51–63, doi:10.5194/acp-4-51-2004, 2004.
- 698 Stephens, M., Turner, N. and Sandberg, J.: Particle identification by laser-induced incandescence in a solid-state
699 laser cavity., *Appl. Opt.*, 42(19), 3726–3736, 2003.
- 700 Stohl, A. and Thomson, D. J.: A Density Correction for Lagrangian Particle Dispersion Models, *Boundary-Layer*
701 *Meteorol.*, 90(1), 155–167, doi:10.1023/A:1001741110696, 1999.
- 702 Stohl, A., Forster, C., Frank, A., Seibert, P. and Wotawa, G.: Technical note: The Lagrangian particle dispersion
703 model FLEXPART version 6.2, *Atmos. Chem. Phys.*, 5(9), 2461–2474, doi:10.5194/acp-5-2461-2005, 2005.



- 704 Stohl, A., Berg, T., Burkhardt, J. F., Fjæraa, A. M., Forster, C., Herber, A., Hov, Ø., Lunder, C., McMillan, W. W.,
705 Oltmans, S., Shiobara, M., Simpson, D., Solberg, S., Stebel, K., Ström, J., Tørseth, K., Treffeisen, R., Virkkunen,
706 K. and Yttri, K. E.: Arctic smoke – record high air pollution levels in the European Arctic due to agricultural
707 fires in Eastern Europe in spring 2006, *Atmos. Chem. Phys.*, 7(2), 511–534, doi:10.5194/acp-7-511-2007, 2007.
- 708 Taylor, J. W., Allan, J. D., Allen, G., Coe, H., Williams, P. I., Flynn, M. J., Le Breton, M., Muller, J. B. A.,
709 Percival, C. J., Oram, D., Forster, G., Lee, J. D., Rickard, A. R., Parrington, M. and Palmer, P. I.: Size-dependent
710 wet removal of black carbon in Canadian biomass burning plumes, *Atmos. Chem. Phys.*, 14(24), 13755–13771,
711 doi:10.5194/acp-14-13755-2014, 2014.
- 712 Thevenon, F., Anselmetti, F. S., Bernasconi, S. M. and Schwikowski, M.: Mineral dust and elemental black
713 carbon records from an Alpine ice core (Colle Gnifetti glacier) over the last millennium, *J. Geophys. Res.*, 114,
714 doi:D17102 10.1029/2008jd011490, 2009.
- 715 Tørseth, K., Aas, W., Breivik, K., Fjæraa, A. M., Fiebig, M., Hjellbrekke, A. G., Lund Myhre, C., Solberg, S.
716 and Yttri, K. E.: Introduction to the European Monitoring and Evaluation Programme (EMEP) and observed
717 atmospheric composition change during 1972–2009, *Atmos. Chem. Phys.*, 12(12), 5447–5481, doi:10.5194/acp-
718 12-5447-2012, 2012.
- 719 Tsyro, S., Simpson, D., Tarrasón, L., Klimont, Z., Kupiainen, K., Pio, C. and Yttri, K. E.: Modeling of elemental
720 carbon over Europe, *J. Geophys. Res.*, 112(D23), D23S19, doi:10.1029/2006JD008164, 2007.
- 721 Venzac, H., Sellegri, K., Villani, P., Picard, D. and Laj, P.: Seasonal variation of aerosol size distributions in the
722 free troposphere and residual layer at the puy de Dôme station, France, *Atmos. Chem. Phys.*, 9(4), 1465–1478,
723 doi:10.5194/acp-9-1465-2009, 2009.
- 724 Vestreng, V., Myhre, G., Fagerli, H., Reis, S. and Tarrasón, L.: Twenty-five years of continuous sulphur dioxide
725 emission reduction in Europe, *Atmos. Chem. Phys.*, 7(13), 3663–3681, doi:10.5194/acp-7-3663-2007, 2007.
- 726 Vignati, E., Karl, M., Krol, M., Wilson, J., Stier, P. and Cavalli, F.: Sources of uncertainties in modelling black
727 carbon at the global scale, *Atmos. Chem. Phys.*, 10(6), 2595–2611, doi:10.5194/acp-10-2595-2010, 2010.
- 728 Wang, M., Xu, B., Kaspari, S. D., Gleixner, G., Schwab, V. F., Zhao, H., Wang, H. and Yao, P.: Century-long
729 record of black carbon in an ice core from the Eastern Pamirs: Estimated contributions from biomass burning,
730 *Atmos. Environ.*, 115, 79–88, doi:10.1016/j.atmosenv.2015.05.034, 2015.
- 731 Wendl, I. A., Menking, J. A., Färber, R., Gysel, M., Kaspari, S. D., Laborde, M. J. G. and Schwikowski, M.:
732 Optimized method for black carbon analysis in ice and snow using the Single Particle Soot Photometer, *Atmos.*
733 *Meas. Tech. Discuss.*, 7(3), 3075–3111, doi:10.5194/amtd-7-3075-2014, 2014.
- 734 van der Werf, G. R., Randerson, J. T., Giglio, L., Collatz, G. J., Kasibhatla, P. S. and Arellano, A. F.: Interannual
735 variability in global biomass burning emissions from 1997 to 2004, *Atmos. Chem. Phys.*, 6(11), 3423–3441,
736 doi:10.5194/acp-6-3423-2006, 2006.
- 737 van der Werf, G. R., Randerson, J. T., Giglio, L., Collatz, G. J., Mu, M., Kasibhatla, P. S., Morton, D. C.,
738 DeFries, R. S., Jin, Y. and van Leeuwen, T. T.: Global fire emissions and the contribution of deforestation,
739 savanna, forest, agricultural, and peat fires (1997–2009), *Atmos. Chem. Phys.*, 10(23), 11707–11735,
740 doi:10.5194/acp-10-11707-2010, 2010.
- 741 World Bank Group, M.: The World Bank Data, 2016.
- 742 Xu, Y., Ramanathan, V. and Washington, W. M.: Observed high-altitude warming and snow cover retreat over
743 Tibet and the Himalayas enhanced by black carbon aerosols, *Atmos. Chem. Phys.*, 16(3), 1303–1315,



744 doi:10.5194/acp-16-1303-2016, 2016.
745 Yoon, J., von Hoyningen-Huene, W., Vountas, M. and Burrows, J. P.: Analysis of linear long-term trend of
746 aerosol optical thickness derived from SeaWiFS using BAER over Europe and South China, Atmos. Chem.
747 Phys., 11(23), 12149–12167, doi:10.5194/acp-11-12149-2011, 2011.
748 Yoon, J., Burrows, J. P., Vountas, M., von Hoyningen-Huene, W., Chang, D. Y., Richter, A. and Hilboll, A.:
749 Changes in atmospheric aerosol loading retrieved from space-based measurements during the past decade,
750 Atmos. Chem. Phys., 14(13), 6881–6902, doi:10.5194/acp-14-6881-2014, 2014.
751 Yttri, K. E., Aas, W., Bjerke, A., Cape, J. N., Cavalli, F., Ceburnis, D., Dye, C., Emblico, L., Facchini, M. C.,
752 Forster, C., Hanssen, J. E., Hansson, H. C., Jennings, S. G., Maenhaut, W., Putaud, J. P. and Tørseth, K.:
753 Elemental and organic carbon in PM10: a one year measurement campaign within the European Monitoring and
754 Evaluation Programme EMEP, Atmos. Chem. Phys., 7(22), 5711–5725, doi:10.5194/acp-7-5711-2007, 2007.
755 Zhou, C., Penner, J. E., Flanner, M. G., Bisiaux, M. M., Edwards, R. and McConnell, J. R.: Transport of black
756 carbon to polar regions: Sensitivity and forcing by black carbon, Geophys. Res. Lett., 39(22), L22804,
757 doi:10.1029/2012gl053388, 2012.
758
759
760
761
762
763
764
765
766
767
768
769
770
771
772
773
774
775
776
777
778
779
780
781
782



783 **Table and figures**

784

785 **Tables**

786 **Table 1. rBC mass concentrations at seasonal resolution and relative increases compared to 1825-1850**
787 **(preindustrial era) for different time periods.**

Time period	Summer		Winter	
	Concentration in $\mu\text{g L}^{-1}$	Relative increase	Concentration in $\mu\text{g L}^{-1}$	Relative increase
	(median \pm SD)	to 1825-1850	(median \pm SD)	to 1825-1850
1825-1850	4.3 \pm 1.5	1.0	2.0 \pm 0.9	1.0
1850-1900	5.3 \pm 2.6	1.1	2.5 \pm 1.4	1.0
1900-1950	7.9 \pm 3.9	1.5	3.2 \pm 1.6	1.4
1950-2000	20.0 \pm 7.1	4.3	6.0 \pm 2.7	2.7
1960-1980	22.6 \pm 7.2	5.0	7.1 \pm 2.5	3.3
2000-2013	17.7 \pm 5.9	3.9	5.4 \pm 2.3	2.4

788

789

790

791

792

793

794

795

796

797

798

799

800

801

802

803

804

805

806

807

808

809

810

811



812 **Figure captions**

813 **Figure 1.** Location of the ice core drilling site (43°20'53, 9°N, 42°25'36, 0°E, 5115 m a.s.l., indicated by the red
814 star or arrow) in the Mt. Elbrus, the western Caucasus mountain range between the Black and the Caspian seas.

815 **Figure 2.** Five regions classified as potential rBC emission sources regions.

816 **Figure 3.** A Profile of high-resolution rBC concentration of Mt. Elbrus ice cores. (a) whole rBC profile of both
817 the 2013 core and the 2009 core, and (b) the 2009 core from top to 20 m corresponding to the blue region in (a).
818 In (b), lower resolution (at ~5-10 cm resolution; black color) and high resolution (at 1 cm resolution; red color)
819 rBC profiles obtained from discrete analysis and continuous flow analysis, respectively, are shown. For a whole
820 rBC record, a section of lower-resolution signals of the 2009 core (corresponding to calendar year 2009) was
821 replaced with the high-resolution rBC signals of the 2013 core. Gray text on top of figures stands for calendar
822 year corresponding to ice core depth.

823 **Figure 4.** Annually averaged temporal evolution in rBC mass concentration of the ELB ice cores. (a) Summer
824 and (b) winter. Thin solid line is medians and dashed lines are lower and upper 10th percentiles of the seasonal
825 rBC values. Upper 10th percentiles do not exceed 75 $\mu\text{g L}^{-1}$ and 35 $\mu\text{g L}^{-1}$ for mid-summer and mid-winter,
826 respectively. Thick lines are 10-year smoothing of medians. Discontinuous thin lines indicate ice layers with
827 unclear seasonality or unanalyzed ice layers. Note different y-scales for seasonal rBC concentrations.

828 **Figure 5.** Time series of mass mode diameter (MMD) of seasonal rBC size distributions for the period of 1940-
829 2009. The MMD was obtained by fitting a log-normal curve to the measured distribution. Horizontal lines stand
830 for geometric means for summer (red) and winter (blue).

831 **Figure 6.** Air mass footprint area for (a) June to August (JJA) and (b) December to February (DJF) in the
832 atmospheric column and (c) JJA in the lowest 2 km in the atmosphere. Color bar on the left indicates footprints
833 density with a process defined unit (p.d.u.). The location of the ELB site is marked by a white triangle. JJA and
834 DJF correspond to summer and winter of the ELB ice core depth, respectively.

835 **Figure 7.** Contribution of each regional footprint density (%) for (a) JJA and (b) DJF in the atmospheric column
836 and (c) JJA in the lowest 2 km in the atmosphere. Footprint density of each region is divided by the footprint
837 density of the entire footprint area (EEU+CEU+WEU+NAF+NAM+Others) and then described in percentage.
838 Information for each region is found in the Sect. 2.4.

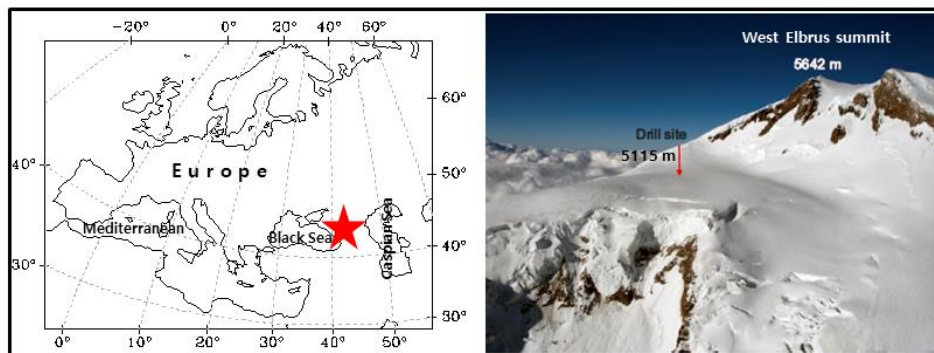
839 **Figure 8.** Historic regional BC emissions and atmospheric BC load at ELB for the period 1900-2008. In (a) and
840 (b), anthropogenic and biomass burning (forest fires and savanna burning) BC emissions estimated by ACCMIP
841 and MACCity (Diehl et al., 2012; Granier et al., 2011; Lamarque et al., 2010; van der Werf et al., 2006). In (c)
842 and (d), atmospheric BC load (Tg yr^{-1}) is calculated by multiplying decadal-scale BC emissions in each region (a
843 and b) by its relative contribution to the entire footprint area of ELB site (figure 7). In (c), both anthropogenic
844 and biomass burning emissions are used for the reconstruction in JJA, as this type of biomass burning (forest
845 fires and savanna burning) is the most frequent in summer and in (d), only anthropogenic emissions are used for
846 DJF. Details are found in the text.

847 **Figure 9.** Comparison in temporal evolution between the rBC mass concentration of the ELB ice core and the
848 estimates of atmospheric BC load at the ELB site, on a decadal scale. (a) JJA and (b) DJF. Best scenarios for
849 atmospheric BC load are shown in black thick lines. In (b), NAM stands for North America. See the text and
850 Figure 8c and d for calculations of the atmospheric BC load.

851



852 **Figures**



853

854 **Figure 1**

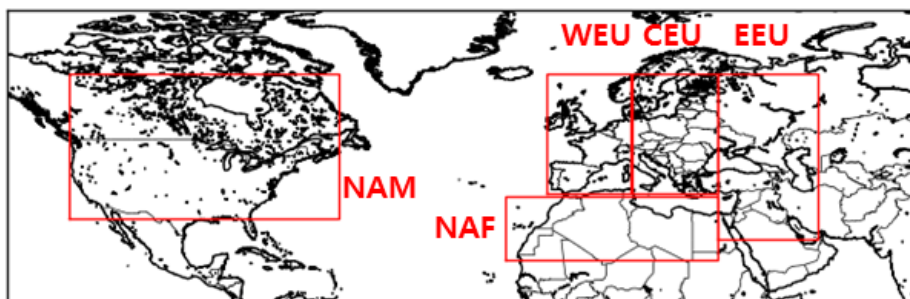
855

856

857

858

859

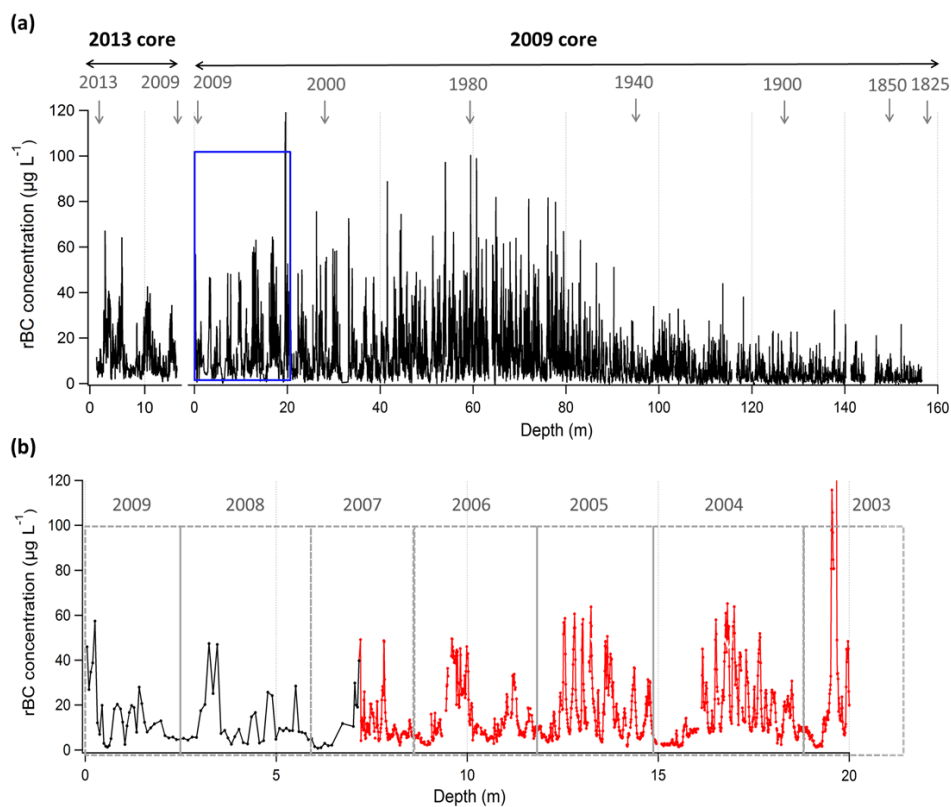


860

861 **Figure 2**

862

863

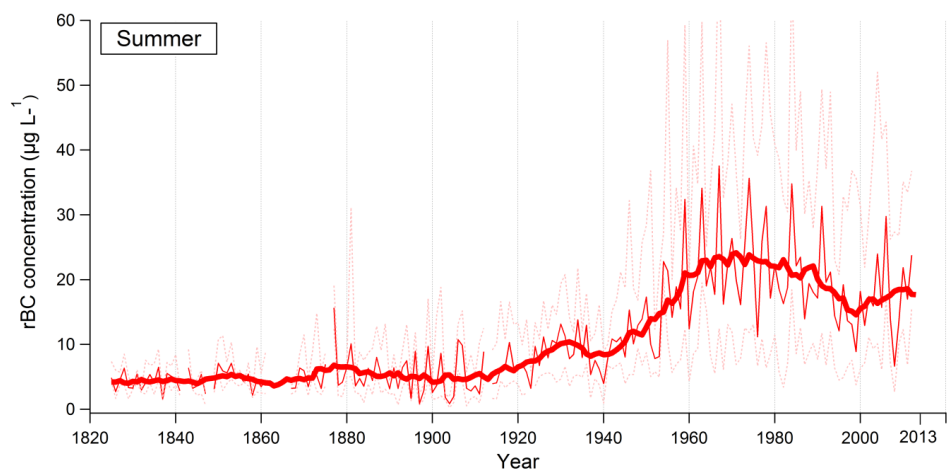


864
865
866
867
868
869
870
871
872
873
874
875
876
877
878
879
880
881
882

Figure 3



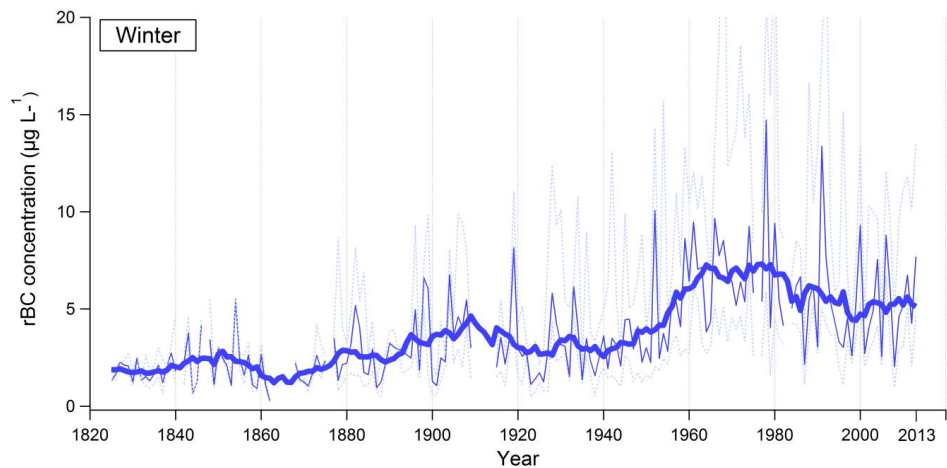
883 (a)



884

885

886 (b)



887

888 **Figure 4**

889

890

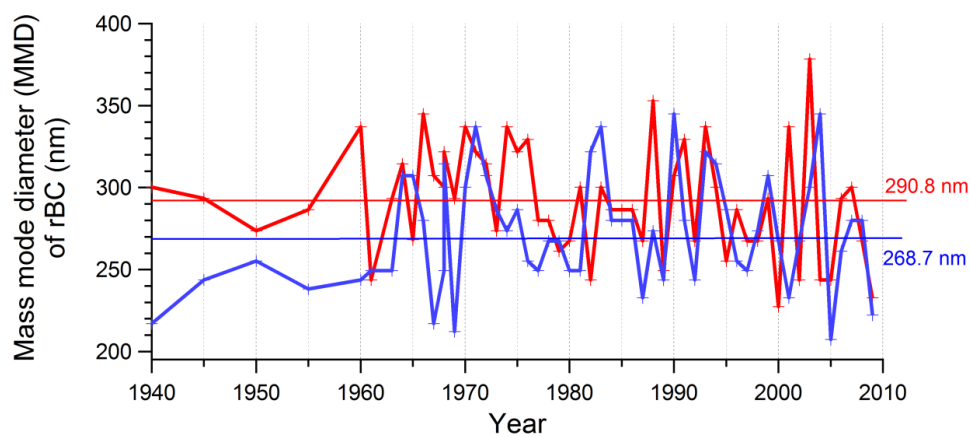
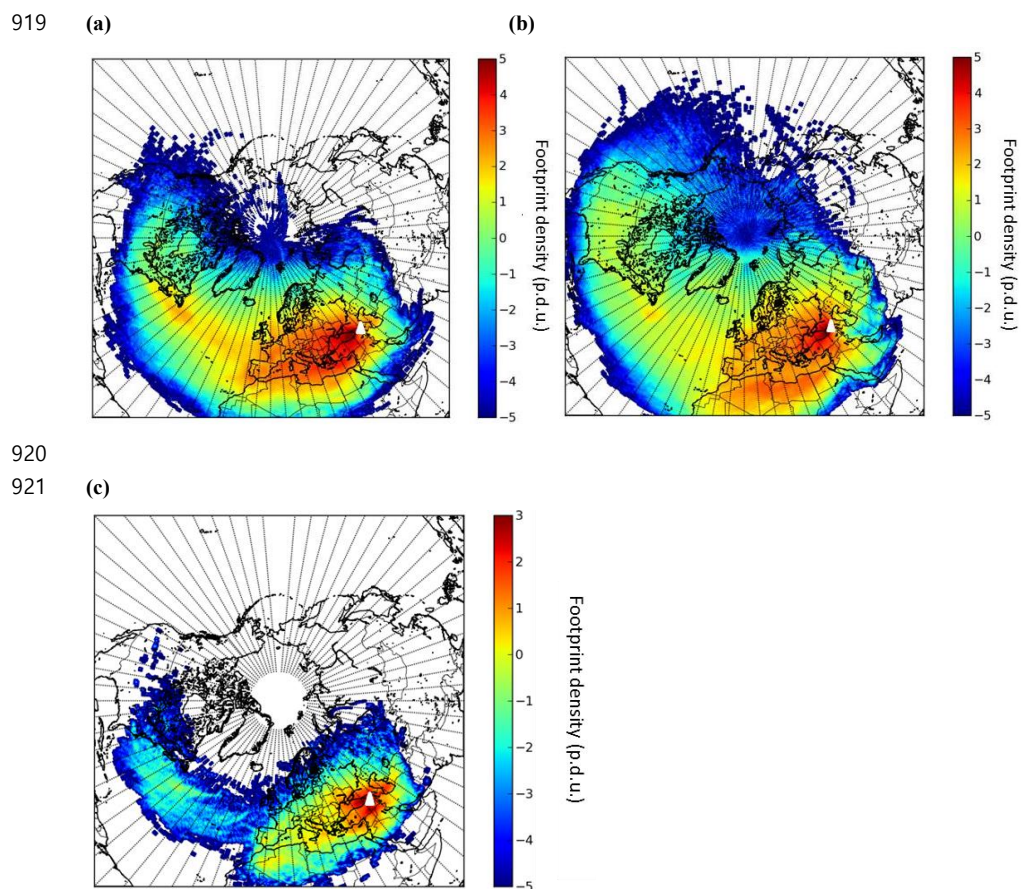


Figure 5

891
892
893
894
895
896
897
898
899
900
901
902
903
904
905
906
907
908
909
910
911
912
913
914
915
916
917
918

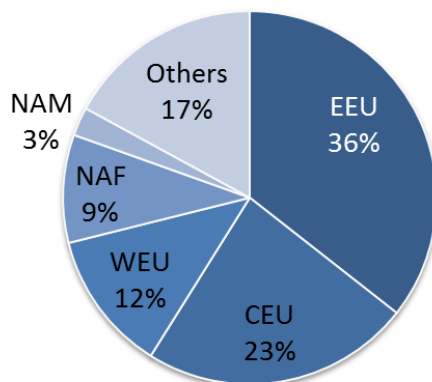


922
923
924
925
926
927
928
929
930
931
932
933
934
935
936
937

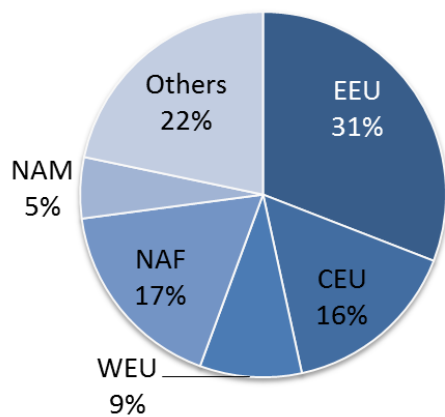
Figure 6



938 (a)



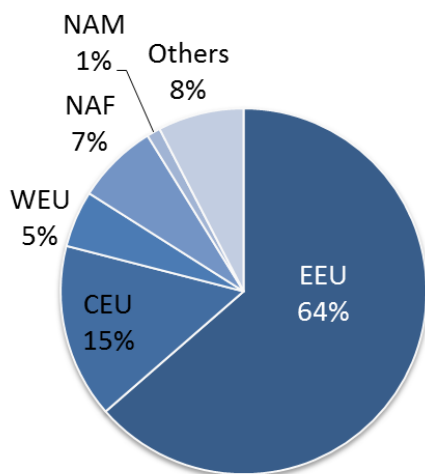
939 (b)



940



941 (e)



942

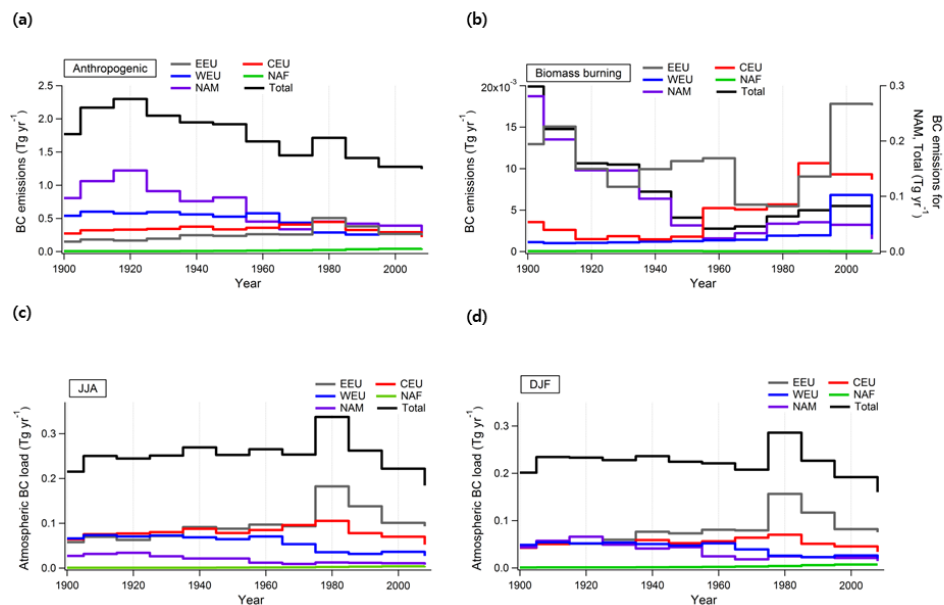
943 **Figure 7**

944

945

946

947



948

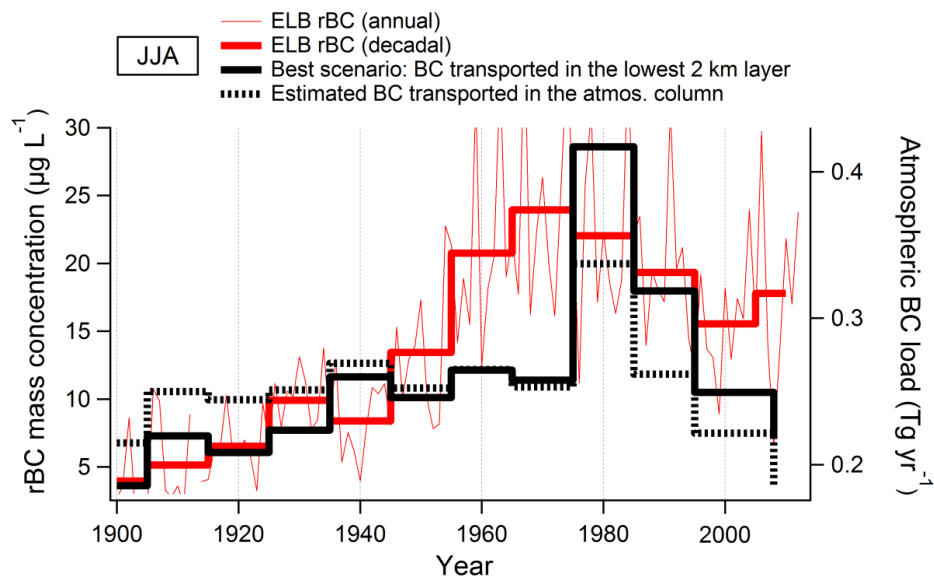
949 **Figure 8**

950

951

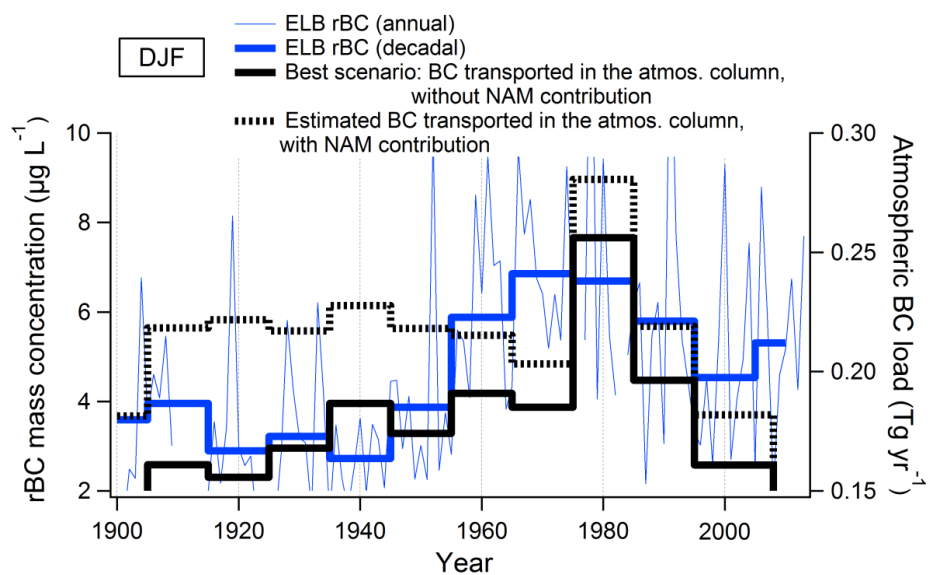


952 (a)



953

954 (b)



955

956 Figure 9

957

958

959

960

961